Acta Materialia Transylvanica 7/1. (2024) 18–23.
DOI: Hungarian: https://doi.org/10.33923/amt-2024-01-04
English: https://doi.org/10.33924/amt-2024-01-04

Investigation of Microhardness of Multiaxially Forged Copper Samples

Zsombor JUHÁSZ,[1] József Bálint RENKÓ[2]

[1] *Budapest University of Technology and Economics, Faculty of Mechanical Engineering, Department of Materials Science and Engineering, Budapest, Hungary, zsombor.juhasz@edu.bme.hu*

[2] *Budapest University of Technology and Economics, Faculty of Mechanical Engineering, Department of Materials Science and Engineering, Budapest, Hungary, renko.jozsef@edu.bme.hu*

Abstract

In engineering practice, high strength materials attract extraordinary attention. Such materials can be produced by many different methods, from which, multiaxial forging was selected. In this work a sum of four samples were compressed by two−directional multiaxial forging. The achieved logarithmic deformation in each step was 0.8 while the accumulative plastic strain of the workpieces were 0.8, 1.6, 2.4, and 3.2. The hardness of the samples was examined in 200 points of measurement on the surface of the mid-section of each to investigate hardening patterns.

Keywords: *severe plastic deformation, multiaxial forging, microstructural analysis.*

1. Introduction

The methods of severe plastic deformation (SPD) are especially suitable for enhancing strength, toughness, and fatigue resistance **[1, 2]**. During SPD, due to the high amount of plastic deformation, an increase in dislocation density will be apparent. This causes an increase in areas surrounded by non-equilibrium grain boundaries. These are the so-called dislocation cells. The emerging structure can be nano (NG) or ultrafine (UFG) grained. The former is made of dislocation cells, where grains differ from each other only by a couple of degrees in their orientation **[3, 4]**. while in the latter, grains are bound by high-angle equilibrium boundaries. These "building blocks" are formed as the dislocation density rises and the borderline dislocations eliminate each other. Differences show in the size as well. The nanograined area is defined on an interval between 10-100 nm, while the UFG territory starts at couple hundred nm and ends at 1 μm **[3, 5]**.

When using the methods of SPD, the aim usually is the creation of UFG structure. Former studies showed that materials, that possess such a structure would be able to endure much higher deformation compared to common, cold rolled steel, along the grain refinement induced increase in strength **[6, 7]**.

When examining the UFG and coarse-grained variation of the same material, UFG will be able to deform almost as much as the latter, while its strength could exceed several times that of the cold rolled state **[7]**.

Though SPD includes several processes this study focuses primarily on multiaxial forging **[8]**.

As a result of our previous research, a closed-die multiaxial forging tool, capable of producing UFG structure, was manufactured **[9]**. Microstructural examinations were conducted on workpieces formed by this tool in the transverse and normal directions. These showed the formation of UFG structure, along with a higher hardness in the middle line of the samples defining a characteristic pattern for each one of them. When moving towards the side of the sample, the increase in hardness shows a declining gradient. This difference is caused by the design of the tool. The sides of the samples that show a lower hardness contact the covers of the die, which resulted in friction hindered deformation despite good lubrication **[10]**.

Our aim with this study was to expand previous findings by examining the longitudinal section of workpieces processed by the same tool on the same deformation spectrum.

2. Experimental

2.1. Material

The material used for the experiments was Cu99.9 industrial grade copper. The material was already at our disposal due to former studies, and the dimensions of the tool were determined so that they could withstand the resulting forces from the sample during the process.

A total of 4 column-shaped workpieces were produced of the chosen material. These had the nominal dimensions of 10×10×20 mm. After manufacturing, the pieces were subjected to heat treatment for 15 minutes at 950 °C, then cooled in water.

2.2. Equipment

A sketch of the closed-die multiaxial forging tool is shown in **Figure 1**. The tool can be divided into three main parts. These are the center block, the tool housing, and the linear actuators. The first one is responsible for positioning the stamps, furthermore it is connected through an intermediate piece to the housing. The latter is to provide a frame embracing the tool, as well as to aid in the tool movements. The main function of the linear actuators is to move the stamps and forward the load to them.

The forming done by the tool is shown in **Figure 2.** It is important to highlight that at any step, only one of the two pairs of stamps is working, while the other is always secured in its position, passively closing die (**Figure 2a**). When finishing a forging step (**Figure 2b**), the ejectors are pushed in, settling back to the initial positioning (**Figure 2c**). Following this, another forging step can be executed, concluding a whole forging cycle (**Figure 2d**).

2.3. Experiment

The forming of the workpieces was done with an MTS 810 type universal material testing machine. The performed forming cycles of the samples were 0.5, 1, 1.5 and 2, respectively. Due to the design of the tool, each forging step caused 0.8 logarithmic plastic deformation. Hence, the cumulative plastic strain was 0.8, 1.6, 2.4 and 3.2, respectively.

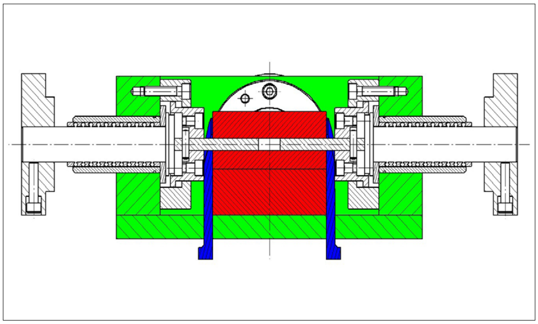

Fig. 1. *Sketch of the multiaxial forging tool. The color markings are as follows: the center block is red, the housing is green, and the ejectors are blue. Uncolored parts (excluding the screws) belong to the linear actuators.*

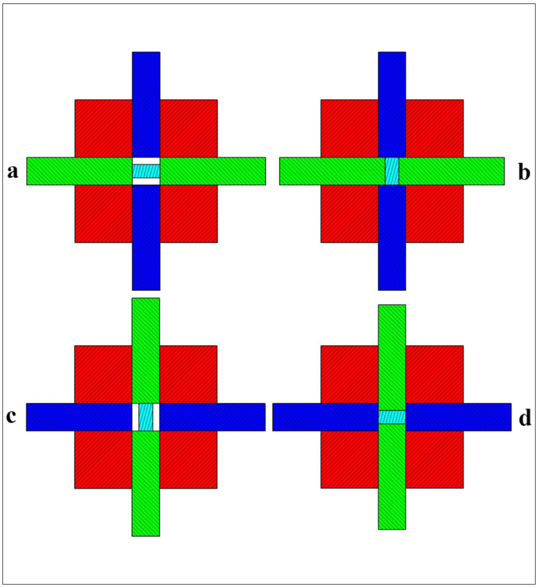

Fig. 2. *Demonstration of one forging cycle. Red shows the housing that positions stamps, the active stamps are blue, while the passive ones are green. The workpiece is turquoise.*

First, as preparation for the metallographic examination, the workpieces were cut on the longitudinal 10×20 mm cross-section along the centerline, parallel to the sides, which came in contact with the covers of the die. The cutting was followed by grinding and polishing. Both steps were performed on a Struers Tegramin-30 type automatic polishing machine. In the last polishing step 1 µm diamond suspension was used with 10 N load on each sample for 8 min.

2.4. Microhardness testing

After the preparation of the samples, microhardness was measured on their surfaces at 200 points. The examination was extended with a virgin (non-deformed) sample for reference. In this case, however, the measurement was performed at only 40 points due to the assumption of isotropic microstructure. The matrix of the measurement points is shown in **Figure 3.** One is for the non-formed sample (a), while the other is for the formed workpieces (b). The outer points of the matrix are 0.5 mm from the edge of both specimens, thus, in the latter case, some points may fall into the resin. These, however, can be easily distinguished since there is a significant difference in the hardness of the resin and the copper.

The measurements were completed using an MCT type programmable microhardness test instrument. This uses the Oliver & Pharr (O&P) method **[11]** for the calculation of hardness, based on the indentation and the load of the piercing tool.

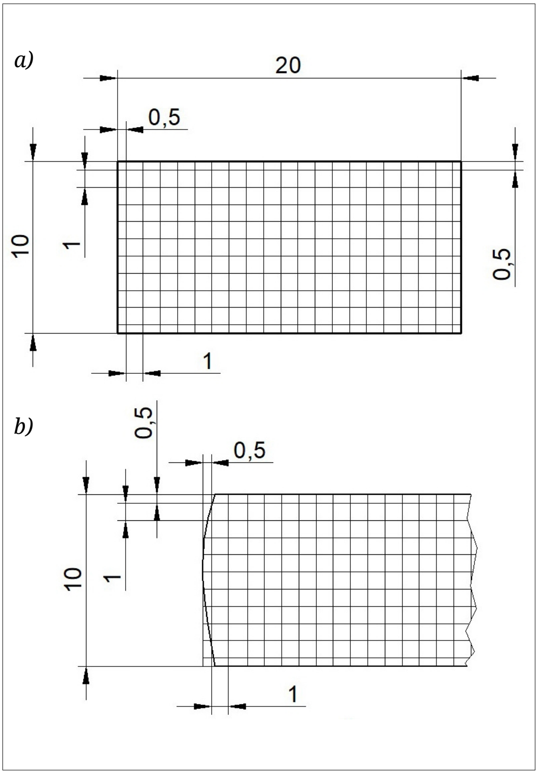

Fig. 3. *Measurement matrix on the virgin (a) and the formed (b) specimens. Every intersection indicates a measurement point.*

3. Results

Based on the measured points, the hardness map of each sample was generated as seen in **Figures 4–8.** The missing points on the maps were artifacts, mostly indented into the resin. The range of the scales was defined globally, so that the different maps could be compared to one another. On the left side of each scale the minimal and maximal hardness value of the measurement belonging to that specific map is presented.

Figure 4 shows that the hardness map is homogeneous, the hardness values on the virgin sample are between 32–65 HV0,5 (avg: 52.6±8,3 HV0,5). This interval is sufficiently narrow, thus, the 40 measurement points are sufficient to represent the hardness of the whole surface. Furthermore, since all the specimens were prepared the same way, their initial state can be assumed isotropic.

The most significant increase in hardness occurred right after the first forging step (**Figure 5**). Although only faintly visible, the characteristic pattern (later visible for each sample) appears as well: a much higher hardness can be observed along the diagonals **[12].** The microhardness here appears between 102.3–177.3 HV0,5.

By the end of the first forming cycle (**Figure 6**) By the end of the first forming cycle.

In the third forming step the interval of the values of hardness narrows down between 124.4–189.6 HV0,5 (**Figure 7**), which indicates a conspicuous rise in hardness on the edges of the specimen. At the same time the widening of the middle, high hardness territory can be observed. This is caused by the hardening of the parts that deform to a higher extent, and therefore, are

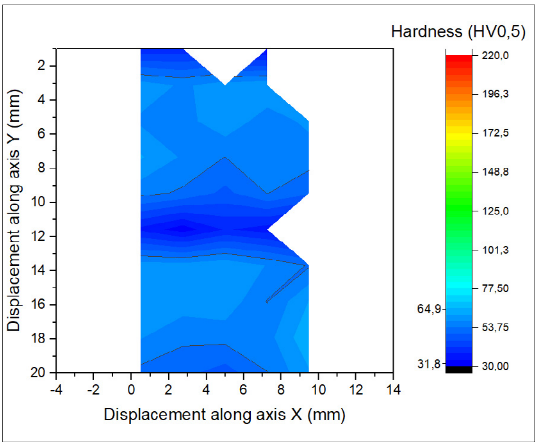

Fig. 4. *Hardness map of the reference specimen.*

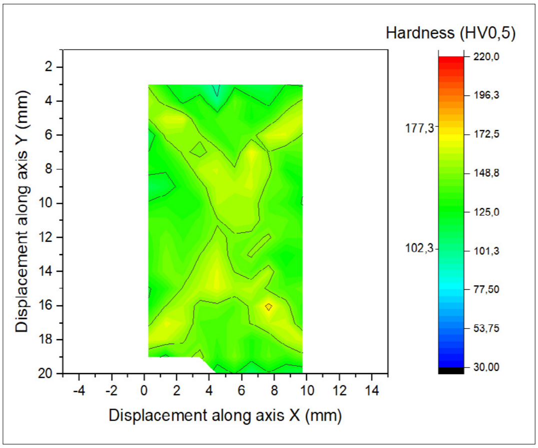

Fig. 5. *Hardness map of the specimen formed for one step.*

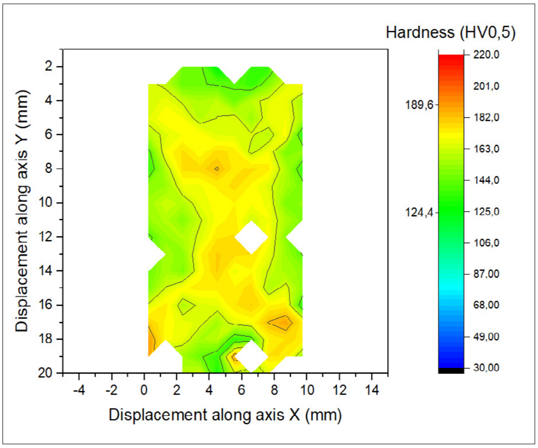

Fig. 7. *Hardness map of the specimen formed for three steps.*

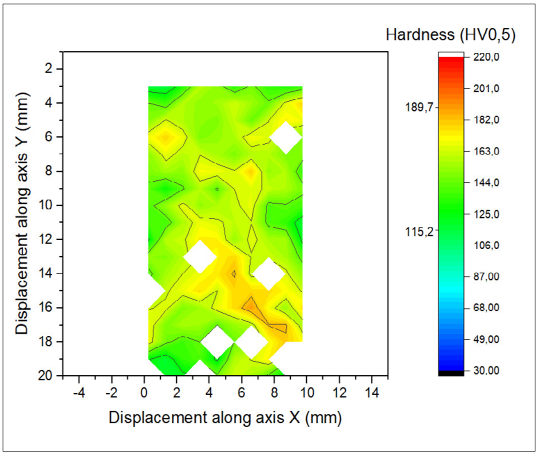

Fig. 6. *Hardness map of the specimen formed for one cycle.*

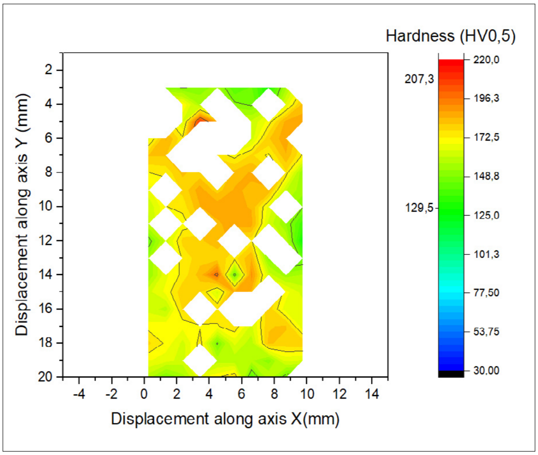

Fig. 8. *Hardness map of the specimen formed for two cycles.*

more resistant to deformation, causing the less deformed parts to gain in on them.

By the end of the second forming cycle (Figure 8), the hardness-interval is pushed and narrowed down. Thus, the hardness values will be between 129.5–207.3 HV0,5. This phenomenon can be experienced in comparison with the third forming step along the diagonals as well. On the edges of the specimen a low hardness zone is separated.

Figures 9–12 show the distribution of the hardness for different steps. Until the third forming step the histograms show a movement in the direction of the higher hardness. By the second forming cycle, the peak stays between 170 HV0,5 and 180 HV0,5, though the interval of distribution narrows down and does not lie as wide as in the third step.

4. Conclusions

It was made clear, that using the O&P method causes significantly more errors to appear than with the use of a manual hardness measuring method. Nonetheless the productivity of this method compensates for the number of errors, for in the time needed to complete the manual examination, several times as many measurements can be completed with the O&P method.

The characteristic cross-shaped pattern along the diagonals is formed because of the friction between the workpiece and the die, despite good lubrication. The friction causes the workpiece at

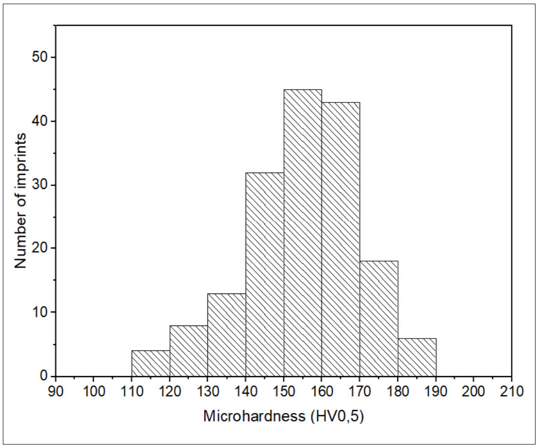

Fig. 9. *The histogram of the hardness values of the first forming step.*

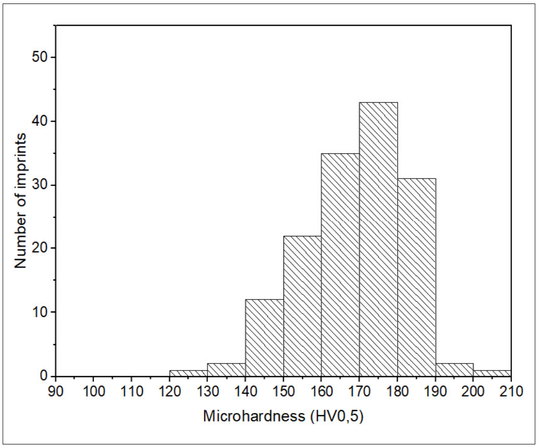

Fig. 11. *The histogram of the hardness values of the third forming step.*

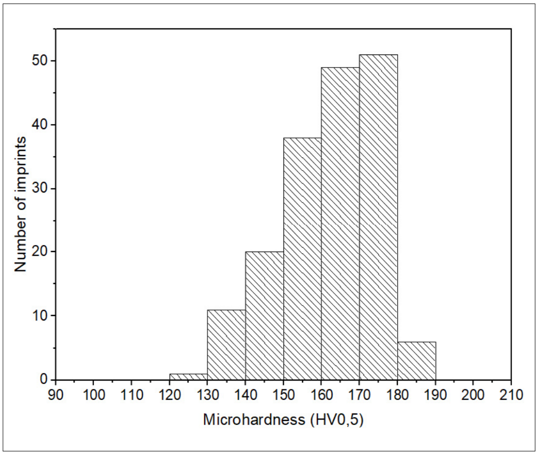

Fig. 10. *The histogram of the hardness values of the first forming cycle.*

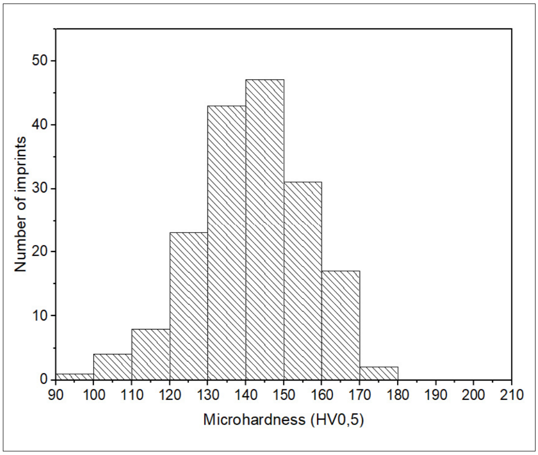

Fig. 12. *The histogram of the hardness values of the second forming cycle.*

these contact areas to stick to the covers, thus reducing the deformation they suffer in these areas, and at the same time inflicting more significant deformation along the diagonals.

Based on **Figures 9–12** the following statement can be made: until the end of the second forming cycle, the hardness rises continuously. This is illustrated through the displacement of the histograms.

Acknowledgement

Supported by the ÚNKP-23-2-I-BME-372 New National Excellence Program of the Ministry for Culture and Innovation from the source of the National Research, Development and Innovation Fund.
The Department of Materials Science and Engineering and the Department of Automotive Technologies of Budapest University of Technology and Economics deserves our special gratitude for providing us the lab equipment necessary for our research, as well as the Institute of Machine Tools and Mechatronics of the University of Miskolc for granting the space and equipment necessary to operate the tool.

References

[1] Langdon T. G.: *The principles of grain refinement in equal-channel angular pressing*. Materials Science and Engineerig A, 462/1–2. (2007) 3–11. https://doi.org/10.1016/j.msea.2006.02.473
[2] Huang Y., Langdon T. G.: *Advances in ultrafine-grained materials.* Materials Today, 16/3. (2013) 85–93. https://doi.org/10.1016/j.mattod.2013.03.004
[3] Siegel R. W.: *Nanophase Materials.* 11. kiadás. VCH Publishers, 1994.

[4] Mughrabi H.: *Dislocation wall and cell structures and long-range internal stresses in deformed metal crystals.* Acta Metallurgica, 31/9. (1983) 1367–1379.
https://doi.org/10.1016/0001-6160(83)90007-X

[5] Chang C. P., Sun P. L., Kao P. W.: *Deformation induced grain boundaries in comercially pure aluminium*. Acta Materialia, 48/13. (2000) 3377–3385.
https://doi.org/10.1016/S1359-6454(00)00138-5

[6] Bereczki P. et al: *Production of ultrafine grained aluminum by cyclic severe plastic deformation at ambient temperature.* In: Institute of Physics, Franciaország, Conf. Ser.: 6th International Conference on Nanomaterials by Severe Plastic Deformation. (2014) 1–11.
https://10.1088/1757-899X/63/1/012140

[7] ValievR. Z.: *Bulk nanostructured materials from severe plastic deformation*. Progress in Materials Science, 45/2. (2000) 103–189.
https://doi.org/10.1016/S0079-6425(99)00007-9

[8] Sakai T., et al.: *Dynamic and post-dynamic recrystallization under hot, cold and severe plastic deformation conditions.* Progress in Materials Science, 60. (2014) 130–207.
https://doi.org/10.1016/j.pmatsci.2013.09.002

[9] Juhász Zs, Bíró T., Renkó J. B.: *Design and Manufacture of closed die multiaxial forging tool.* In: Institute of Physics, Hungary, Conf. Ser.: Mater. Sci. Eng. 1246. (2022) 1–7.
https://doi.org/10.1088/1757-899X/1246/1/012009

[10] Juhász Zs.: *Zárt üregű többtengelyű kovácsolással alakított réz próbatestek mikroszerkezeti vizsgálata.* Szakdolgozat. BME Anyagtudomány és Technológia Tanszék 2022.

[11] Oliver W. C., Pharr G. M.: *Measurement of hardness and elastic modulus by instrumented indentation: Advances in understanding and refinements to methodology.* Journal of Materials Research, 19. (2003) 3–20.
https://doi.org/10.1557/jmr.2004.19.1.3

[12] Juhász Zs.: A t*öbbtengelyű kovácsolás mikroszerkezeti hatásainak vizsgálata.* TDK-article. BME Department of Materials Science and Engineering, Budapest, 2022.